Available online at www.sciencedirect.com

jmr&t Journal of Materials Research and Technology

www.jmrt.com.br

Original Article

XRD, internal field-NMR and Mössbauer spectroscopy study of composition, structure and magnetic properties of iron oxide phases in iron ores

Mushtagatte Manjunatha[a], *Rajeev Kumar*[b], *Aroli V. Anupama*[b], *Vijay B. Khopkar*[b], *Ramakrishna Damle*[a], *Karalapura P. Ramesh*[c,*], *Balaram Sahoo*[b,*]

[a] *Department of Physics, Bangalore University, Bangalore 560056, India*
[b] *Materials Research Centre, Indian Institute of Science, Bangalore 560012, India*
[c] *Department of Physics, Indian Institute of Science, Bangalore 560012, India*

ARTICLE INFO

Article history:
Received 29 August 2018
Accepted 25 January 2019
Available online 11 April 2019

Keywords:
Iron ores
Phase composition
Magnetic properties
Internal field NMR
Mössbauer spectroscopy

ABSTRACT

We report the phase-composition, structure and magnetic properties of two representative samples of naturally available iron-oxide containing ores/soils collected from two different regions in Karnataka, India. Presence of elements such as Fe, Si, Al and O were identified in both the samples using energy dispersive analysis of X-rays (EDAX). X-ray diffraction results confirmed that different ceramic phases such as crystalline iron oxide phases (Fe_3O_4, γ-Fe_2O_3 and α-Fe_2O_3), aluminosilicates (Al_2SiO_5) and low-quartz (SiO_2) phases constitute the soil. The presence of ferrimagnetic phases (Fe_3O_4, γ-Fe_2O_3) makes the soil respond to a permanent magnet. Separation between the magnetic and non-magnetic phases was performed using a permanent magnet. The non-magnetic part of the sample contains a high amount of α-Fe_2O_3 phase along with aluminosilicates and low-quartz. The magnetic phases were further characterized and quantified. The presence of Fe_3O_4 phase in the samples was confirmed from the Verwey transition observed by internal-field NMR spectroscopy. Our results demonstrate that internal-field NMR and Mössbauer spectroscopy are complementary tools for characterizing iron containing soils. Furthermore, we found that the soil collected from the low temperature region (Sandur) contains more amounts of ferrimagnetic oxide (Fe_3O_4, γ-Fe_2O_3) phases, whereas the high temperature region (Hospete) contains more α-Fe_2O_3 phase. Hence, our results confirm that the phase composition of the soil is intimately related to the local daily temperature.

* *Corresponding authors.*
E-mails: kpramesh@iisc.ac.in (K.P. Ramesh), bsahoo@iisc.ac.in (B. Sahoo).
https://doi.org/10.1016/j.jmrt.2019.01.022

1. Introduction

Hematite and magnetite are the primary iron ores used for the extraction of metallic iron by the steel industries. Iron ores that are used by the steel industry requires to contain ≥58 wt% iron compounds, such as iron oxides before being considered as commercially usable [1]. Apart from extraction of metallic iron, the iron oxides (Fe_3O_4, α-Fe_2O_3 and γ-Fe_2O_3) have numerous direct applications, such as in electromagnetic interference shielding [2–4], magnetorheology [5,6], magnetic recording [7], high frequency optical modulators [8] and biomedical applications [9,10] etc.

The analysis of the characterization results of different minerals and their development provides enormous information about understanding of the changes of the minerals through different natural processes [11,12]. Due to the invention of various advanced scientific techniques, the in-depth characterization of various unknown minerals in terms of their elemental and phase composition became feasible. There are many reports on the study of iron ores in different parts of world. For example: Longworth et al. conducted Mössbauer spectroscopic study on the magnetic state of iron oxides in the soils collected from the regions around England [13]. They found that the percentage of non-magnetic compound in the soils varies between 50% and 63%. Resende et al. reported on the iron oxide ores found in the tropical regions of Brazilian soils that contains ~63% of hematite ore [14] and Farbis et al. reported that the Brazilian soils also contain higher amount (~17%) of magnetite [15]. The iron soils collected from the New Zealand contains almost 20–40% of magnetite [16].

There are many parameters such as temperature, quality of air, pressure below the ground etc. that decide the retention of the amount of different iron oxide phases in soils. Furthermore, there are many environmental parameters or combination of parameters such as temperature, mechanical pressure (below earth crust), moisture, oxygen gas (air) along with many other pollutants that influence the transformation of elemental iron/iron-oxide into other iron oxide phases. The aim of this study is to demonstrate the influence of local daily temperature and moisture (due to rain in the forest areas) on the iron oxide phase transformation in the soils collected from two nearby places in Karnataka, India, where the local daily temperatures differ by about 2 °C.

2. Materials and methods

Two different representative soils were collected from two different regions (Hospete and Sandur) in Karnataka, India. These cities are situated at about 350 km toward north of Bangalore, India. They are not more than ~30 km apart from each other. All over the year, Hospete experiences about 2 °C higher temperature than Sandur. This temperature difference could be due to the fact that Hospete has much more dry-land than Sandur, which include forest regions. The virgin soil samples collected from Hospete and Sandur regions were labeled as HS and SS, respectively. To assess the composition and properties of the samples a host of complex characterizations were performed. Initially, the as-collected samples were ground to fine powders. The elemental composition and morphological characterizations of the samples were performed using the techniques like Energy Dispersive Analysis of X-rays (EDAX) (Zeiss, Germany), X-ray diffraction (XRD) (PANAlytical, UK), Scanning Electron Microscope (SEM) (Zeiss, Germany) and Vibrating Sample Magnetometry (VSM) (Quantum Design, USA). The samples were found to be strongly magnetic, as they show strong attraction to a magnet during preliminary assessment. After initial characterizations, the magnetic particles were separated from the original soil via a permanent magnet of maximum field strength of ~1 T. The fraction of the magnetic particles of the sample was about 64% and 68% for HS and SS samples, respectively (i.e., the non-magnetic part was about 36% and 32% for HS and SS samples, respectively). The non-magnetic samples obtained after the magnetic separation were labeled as HS1 and SS1 for Hospete and Sandur soils, respectively, whereas the magnetic samples obtained after the separation were labeled as HS2 and SS2, respectively. The presence of different crystalline phases in all the samples was identified using XRD. The structural and magnetic properties of HS2 and SS2 samples were studied using XRD, ^{57}Fe internal field nuclear magnetic resonance (IFNMR) spectroscopy, ^{57}Fe Mössbauer spectroscopy, X-ray photoelectron spectroscopy (XPS) (AXIS ULTRA, UK) and VSM.

XRD patterns of the samples were collected using *PANalytical X'Pert Pro* diffractometer (Cu-K_α radiation). The crystalline phases present in the soil samples were identified by referring to the Bragg positions and their relative intensities. Rietveld refinements [17] of the structural parameters were carried out using the computer program *FullProf* [18]. The crystallographic information for the refinement was obtained from standard crystallographic information files (*CIF*) from *ICSD* database. ^{57}Fe-Mössbauer spectroscopy was carried out in transmission mode at RT (using SEE Co. USA instrument). The spectra were recorded using a gas-filled proportional counter. The velocity of the drive was calibrated using α-Fe foil at RT. The obtained Mössbauer spectra were least square fit using "*NORMOS*" program [19,20]. The M-H loops of the samples were recorded at RT using a "*PPMS 9T*" magnetometer.

A home-made pulsed IFNMR spin echo spectrometer with two "equal pulse sequences" [21] was used for the measurement of the samples at RT and at 77 K. A detailed description and working principle of the IFNMR instrument is provided elsewhere [22]. In a typical room temperature experimental setup, a LC parallel probe was excited with a pulse sequence of '$\pi/2$–τ–$\pi/2$' (two equal pulses sequence). For the two equal pulses, an optimized pulse width of 1 μs was used as the $\pi/2$ pulse, for which the echo amplitude was the highest. The $\pi/2$ pulse was followed by a delay time τ of 20 μs before arrival of the second $\pi/2$ pulse (1 μs). For low temperature (77 K) experiment, we used a specially designed coaxial probe. The pulse-widths of the two equal pulses were also kept constant even at 77 K. However, the delay between the two pulses was increased to 30 μs, in order to accommodate longer spin–spin relaxation time at low temperature. The echo amplitude (NMR signal) was recorded as a function of frequency varying from 65 MHz to 80 MHz in steps of 0.1 MHz.

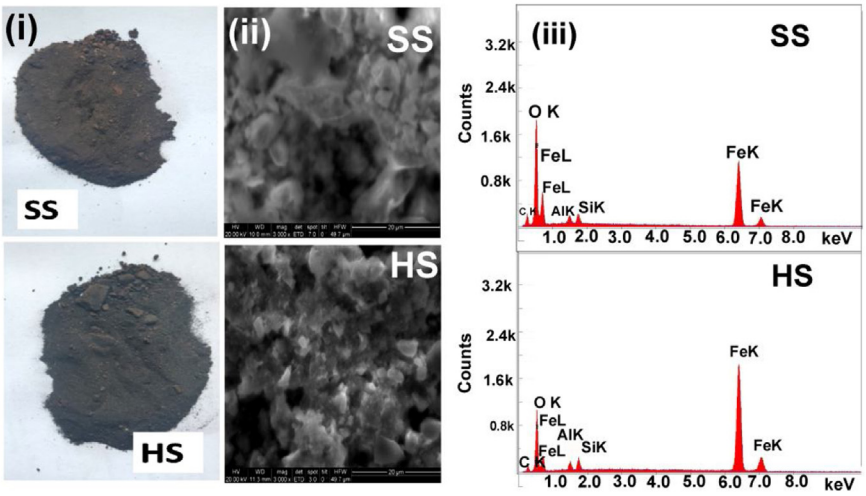

Fig. 1 – (i) The photographs of the as-collected soil samples collected from Sandur (SS) and Hospete (HS). (ii) SEM images of the HS and SS samples. (iii) EDAX spectra of the HS and SS samples.

Table 1 – Elemental composition obtained from EDAX experiment.

Soil Sample	Elements	Atomic %
HS	O	57.97
	Al	3.60
	Si	3.50
	Fe	34.93
SS	O	79.01
	Al	2.18
	Si	3.65
	Fe	15.16

3. Results and discussion

3.1. *Samples before separation of the magnetic phases*

The photographs of the as-collected HS and SS samples are shown in Fig. 1(a). The Hospete soil (HS) is dark brown in color whereas the Sandur soil (SS) is brownish. This suggests that both the soils contain high amount of iron oxide phases. Fig. 1(b) shows the SEM micrographs of HS and SS samples, respectively. The irregular structural morphology of the particles in the soils is evident from the SEM micrographs of both the samples. Fig. 1(c) shows the EDAX spectra for HS and SS samples, respectively. Both the samples contain Fe, Si, Al and O as major elements. The elemental composition of both the soil samples (HS and SS) obtained from EDAX is listed in Table 1.

As the amount of these elements largely depends on sampling area of the sample, we cannot conclude on the accuracy of elemental composition. However, it seems that HS contains higher percentage (34.93 at%) of Fe than that of SS (15.16 at%). However, both the samples contain oxygen as the most abundant element (57.96 at% for HS and 79.01 at% for SS). Presence of these two major elements indicates that both the samples contain high amount of iron oxide phases (α-Fe_2O_3, Fe_3O_4 and γ-Fe_2O_3) as supported by the XRD results discussed below. Assigning appropriate (stoichiometric) amount of oxygen to the aluminosilicate (4–5 mol%, Al_2SiO_5) and low-quartz (2–3 mol%, SiO_2) phases, a simple calculation suggests that there are oxygen deficient regions (oxygen vacancies) present in the samples. It can be rationalized from Table 1 that HS sample contains more oxygen deficient iron containing phases than the SS sample. The XRD patterns of HS and SS samples are shown in Fig. 2(a). The XRD patterns indicate that samples contain iron oxides (α-Fe_2O_3, Fe_3O_4 and γ-Fe_2O_3) as major phases along with small amounts of aluminosilicates and quartz. The M–H loops for the HS and SS samples are shown in Fig. 2(b). It is clear that HS sample has saturation magnetization (M_S) of ~8 emu/g whereas SS sample shows an M_S value of ~19 emu/g. This confirms that SS sample is slightly more magnetic as compared to HS sample.

3.2. *Samples after removal of the non-magnetic phases*

After grinding the as collected samples to fine powders, the magnetic part of both the samples were separated from the non-magnetic/weakly magnetic parts. However, as the particles sizes were still bigger, presence of small magnetic grains in the non-magnetic matrix and vice versa, cannot be ruled out. The non-magnetic part of the samples obtained after the magnetic separation were labeled as HS1 and SS1 for Hospete and Sandur soils, respectively. Similarly, the magnetic parts of the samples were labeled as HS2 and SS2. After the magnetic separation we have further collected the XRD patterns of both the magnetic and non-magnetic parts of both the samples. Fig. 3(a) shows the XRD patterns of all the samples measured after the magnetic separation. It can be seen that non-magnetic phases like aluminosilicates and quartz are prominent over the magnetic phases. Different crystalline forms of aluminosilicates present in the samples are identified as Kyanite (Space-group: $P\bar{1}$) and Sillimanite (Space-group: *Pnma*), as given in Fig. 3(a). The soils contain mostly aluminosilicates and quartz as the non-magnetic phases.

To understand the effect of daily environmental temperature on the phase composition and phase transformation

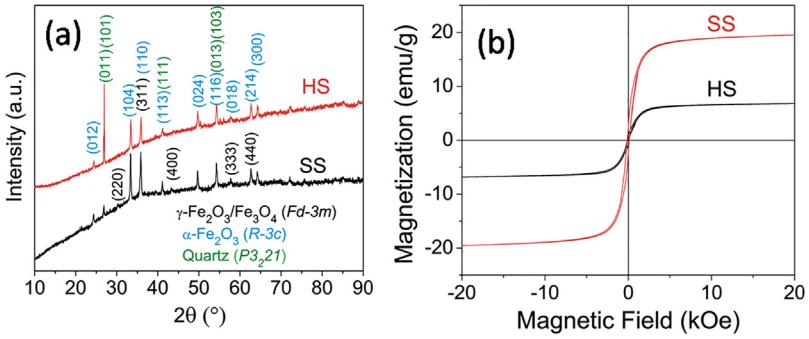

Fig. 2 – (a) XRD patterns for the soil samples HS and SS. (b) M–H loops of the studied soil samples: HS (black) and SS (Red), measured at RT.

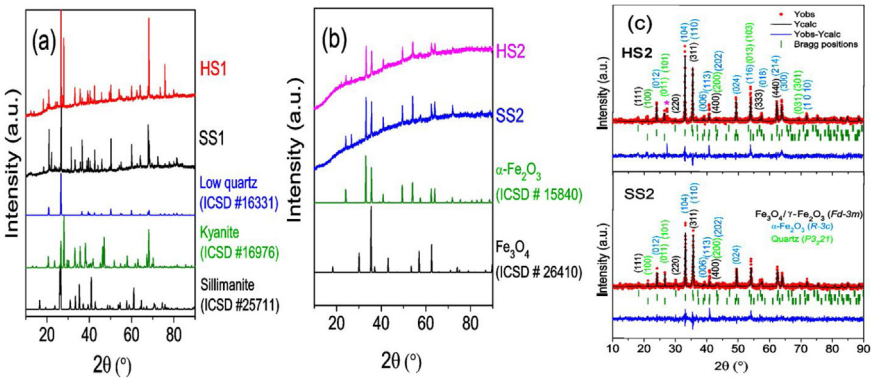

Fig. 3 – The XRD patterns of the soil samples: (a) HS1 and SS1, (b) HS2 and SS2. For identification purposes standard (ICSD) XRD patterns of the observed phases are also shown. (c) The Rietveld refined XRD patterns for the soil samples. The data points in red circles, black lines and blue lines (below XRD pattern) represent the experimental data, fit to the experimental data and the difference pattern (mismatch between experimental data and refined data), respectively. The vertical bars below the XRD patterns (in green color) represent Bragg positions.

Table 2 – The Rietveld refined XRD parameters. The abbreviations '*a*' and 'V' stand for the unit cell parameter and cell volume, respectively. The error in estimation of '*a*' is in the 4th decimal.

Sample	Phase (wt%) space group	Cell parameters (Å), volume (Å^3)
HS2	Fe_3O_4/γ-Fe_2O_3 (5.3 ± 0.5) [*Fd-3m*]	*a* = 8.4077, V = 594.3
	α-Fe_2O_3 (81.5 ± 1.3) [*R-3c*]	*a* = 5.0364, *c* = 13.7541, V = 302.13
	Low quartz (13.2 ± 1.0) [$P3_221$]	*a* = 4.8365, *c* = 5.5604, V = 112.64
SS2	Fe_3O_4/γ-Fe_2O_3 (20.9 ± 1.0) [*Fd-3m*]	*a* = 8.3775, V = 587.95
	α-Fe_2O_3 (71.1 ± 1.2) [*R-3c*]	*a* = 5.0329, *c* = 13.7451, V = 301.52
	Low quartz (8.0 ± 0.6) [$P3_221$]	*a* = 4.8186, *c* = 5.5682, V = 111.97

behavior, the magnetic part of the samples were studied extensively. The XRD patterns of the magnetic part of the soil samples (HS2 and SS2) show presence of Fe_3O_4/γ-Fe_2O_3 (*Fd-3m*), α-Fe_2O_3 (*R-3c*) and low quartz ($P3_221$) phases (Fig. 3(b)). The Rietveld refined XRD patters are shown in Fig. 3(c). The major Bragg reflections are indexed in Fig. 3(c) and the indices of individual phases are color-coded for clarity. From the Rietveld refinement results (Table 2), we observe that both the samples (after separation by a magnet) still contain α-Fe_2O_3 as the major phase, i.e., ~81% for HS2 and ~71% for SS2 samples. However, the amount of magnetic phase (Fe_3O_4/γ-Fe_2O_3) is estimated to be ~5.3 ± 0.5 wt% for HS2 and ~20.9 ± 1.0 for SS2 samples, i.e., the SS2 sample contains more amount of magnetic phase than HS2 sample. Also, the total amount of iron oxide phases (Fe_3O_4/γ-Fe_2O_3 + α-Fe_2O_3) is higher in SS2 than HS2 sample (Table 2). There are small quantities of the non-magnetic low-quartz (SiO_2) phase still present in both the samples (~13 wt% in HS2 soil and 8 wt% in SS2 soil). Note that, although the Bragg positions correspond to *Fd-3m* structure of Fe_3O_4 phase, γ-Fe_2O_3 can also assume *Fd-3m* structure [23]. Hence, quantification of the magnetic part into Fe_3O_4 and γ-Fe_2O_3 phases, by XRD alone, is not possible, unless γ-Fe_2O_3 possesses $P4_332$ structure [24,25]. However, it is known that γ-Fe_2O_3 or defected-Fe_3O_4 (Fe^{2+} partially oxidized to Fe^{3+}) usually has lower lattice parameter than the Fe_3O_4 phase [23,25,26]. Interestingly, in case of HS2, the cell parameter (*a*) is 8.4077 Å, while that for SS2 is 8.3775 Å. This suggests that SS2 might contain defected-Fe_3O_4 as prominent phase. In case of

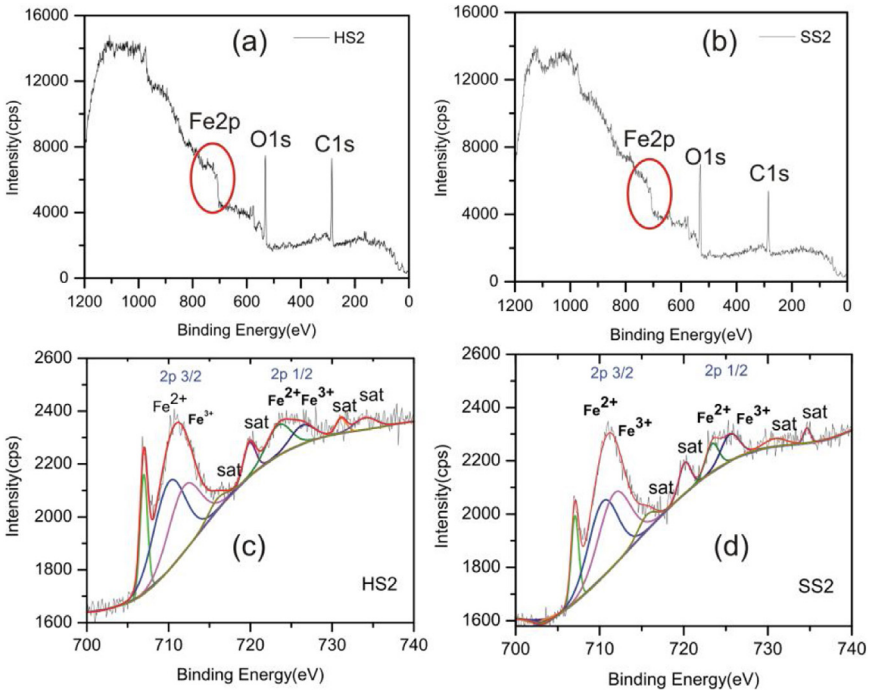

Fig. 4 – The XPS spectra of (a) HS2 and (b) SS2 samples over the whole measured energy range. The Fe2p XPS spectra of (c) HS2 and (d) SS2 samples.

both the samples, a slight misfit at a few diffraction angles (and an unaddressed peak at ~27.5° (marked as asterisk) for HS2 sample) correspond to the aluminosilicates in the soil samples. However, the abundance of this phase is <2 wt% in the whole sample.

Fig. 4(a, b) shows the XPS spectra of the two soil samples (HS2 and SS2). The Fe2p and O1s peaks are well pronounced along with the C1s peak (due to the carbon tape used during the measurement). The Fe2p XPS spectra of the HS2 and SS2 samples were further measured with better energy resolution and are shown in Fig. 4(c, d). It is clear that, the binding energy for the iron lies between 700 and 735 eV. The intense peak, which appears around 710 eV, confirms the presence of Fe^{2+} ($Fe2P_{3/2}$) in both the samples. The peak at ~713 eV corresponds to Fe^{3+} ($Fe2P_{3/2}$). The satellite peaks corresponding to Fe^{2+} and Fe^{3+} appear in the range ~715–722 eV. The peaks seen at ~724 eV and ~728 eV correspond to the $Fe^{2+}$and Fe^{3+} ions ($Fe2P_{1/2}$), respectively. The peaks observed in the range ~730–736 eV correspond to the satellite lines of Fe^{2+} and Fe^{3+} ions ($Fe2P_{1/2}$). The XPS results corroborate the XRD results that both Fe^{2+} and Fe^{3+} ions are present in the sample, i.e., α-Fe_2O_3, Fe_3O_4 and γ-Fe_2O_3 phases are present in both the samples. The peak observed at ~708 eV gives the impression that metallic iron (Fe^0) might be present in both the samples. However, we have not observed any trace of metallic Fe phase in any of the characterization methods reported here. Earlier, a similar peak was observed for low spin Fe^{2+} state [27–29]. The origin of low spin Fe^{2+} state can be due to the presence of high amount of defects in the samples as indicated from the EDAX measurements (Table 1). Hence, this peak may correspond to the same low spin 2+ oxidation state of Fe.

The Mössbauer spectra of both the samples measured at RT are given in Fig. 5. Keeping the XRD results in mind, that both the samples contain Fe_3O_4, α-Fe_2O_3 and γ-Fe_2O_3 phases, and each spectrum was fit with four sub-spectra shown as four sextets in Fig. 5(a). All the Mössbauer parameters obtained from the least-squares fitting are listed in Table 3. All the isomer shift (IS) values are given with respect to the ^{57}Co source (Rh-matrix) at RT. The dominant sextet (S1) seen in both samples (dark green color, $B_{hf} = 51.5$ T) is assigned to the α-Fe_2O_3 phase [25]. The sextet (S2) shown in green color ($B_{hf} = 49.7$ T) is assigned to the γ-Fe_2O_3 phase. The other two additional sextets having $B_{hf} = 48.9$ T (S3) and 45.9 T (S4) are assigned to the A and B sites of Fe_3O_4 phase, respectively. A singlet (P) corresponding to paramagnetic phase is also observed in both the samples, which might be due to the presence of some Fe atoms in the non-magnetic phase [9]. Clearly, the HS2 sample contains more α-Fe_2O_3 phase. A comparison between the area% obtained for α-Fe_2O_3 and for the ferrimagnetic phases (γ-Fe_2O_3 and Fe_3O_4) suggests that the fraction of α-Fe_2O_3 content in HS2 is much higher than SS2 sample.

Fig. 5(b) shows the M versus H loops for HS2 and SS2 samples. The samples (the magnetic parts) show saturation magnetization (M_S) of ~16 emu/g and ~22 emu/g for HS2 and SS2, respectively. As seen earlier, the M_S value for HS and SS samples were 8 emu/g and 19 emu/g, respectively (Fig. 2(b)). Hence, the saturation magnetization values for the magnetic part of the samples increased only slightly for SS2 sample, but considerably for HS2 sample. However, the saturation magnetization values are not quite similar to the M_S values of Fe_3O_4 and γ-Fe_2O_3 phase [29–33]. This suggests that the separation of magnetic and non-magnetic parts is not ideal.

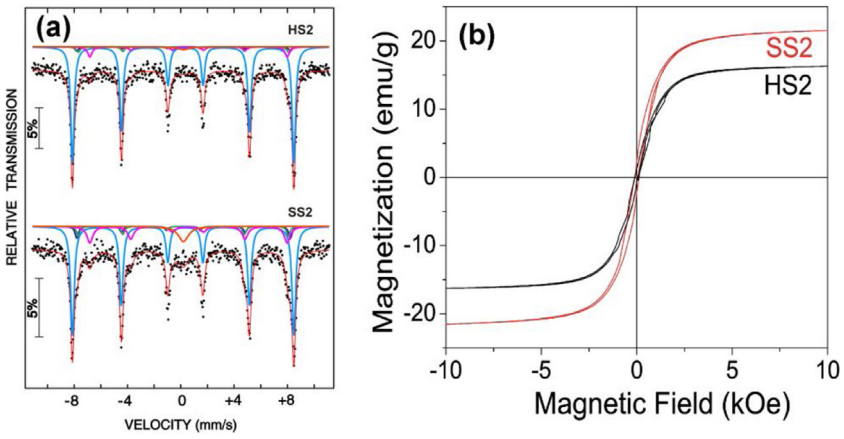

Fig. 5 – (a) The ^{57}Fe Mössbauer spectra of both the samples (HS2 and SS2) measured at RT. (b) Magnetization loops for HS2 and SS2 samples, measured at RT.

Table 3 – Mössbauer spectral parameters obtained from the least square fitting of the Mössbauer spectra of the HS2 and SS2 samples. IS, isomer shift (with respect to ^{57}Co-source (Rh-matrix)); 2ε, quadrupole nuclear level shift; B_{hf}, magnetic hyperfine field; Area%, percent area under the sub-spectrum. The estimated error in the value of each quantity is also given.

Sample	Phase	Sub-spectra	IS (mm/s) ± 0.005	2ε (mm/s) ± 0.005	B_{hf} (T) ± 0.5	Area% ± 2%
HS2	α-Fe_2O_3	S1	0.027	−0.179	51.5	83.88
	γ-Fe_2O_3	S2	0.020	0.002	49.7	2.63
	Fe_3O_4 (A site) (B-site)	S3 S4	0.200 0.560	−0.020 0.05	48.9 45.9	4.38 7.59
	Paramagnetic	P				1.52
SS2	α-Fe_2O_3	S1	0.027	−0.167	51.5	66.20
	γ-Fe_2O_3	S2	0.020	0.002	49.7	5.83
	Fe_3O_4 (A site) (B-site)	S3 S4	0.200 0.560	−0.020 0.050	48.9 45.9	5.5716.28
	Paramagnetic	P				6.12

The IFNMR is a technique to assess the magnetic properties of ferromagnetic and ferrimagnetic materials [21, 34-36]. In a typical IFNMR experiment the transition of nuclear spins between $m_I = +½$ and $m_I = -½$ state is governed by an RF pulse, which creates a resonance condition. The condition for resonance is given by $\omega = \gamma H_{int}$, where ω is the precession frequency of the nuclear spins and also the matching frequency of the RF pulse, γ is the gyromagnetic ratio of ^{57}Fe nucleus ($\gamma = 1.382$ MHz/T), H_{int} is same as the magnetic hyperfine field (B_{hf}) experienced by the NMR active nucleus. From the elemental analysis and the Mössbauer studies it is clear that both of our samples (HS2 and SS2) contain γ-Fe_2O_3 and Fe_3O_4 as major ferrimagnetic phases in its composition. As discussed in the Mössbauer spectroscopy results, the magnetic hyperfine field of these two phases (γ-Fe_2O_3 and Fe_3O_4) varies between 48 and 52 T at RT and between 50 and 55 T at 77 K, which matches with many other previous reports [29,37–41]. These B_{hf} values correspond to an NMR frequency between 60 and 72 MHz at RT and between 65 and 76 MHz at 77 K. As expected, α-Fe_2O_3 phase being antiferromagnetic, no signal was observed at both measurement temperatures (RT and 77 K). The obtained IFNMR results for both the studied samples (HS2 and SS2) are discussed below.

The IFNMR spectra for both the samples (HS2 and SS2) measured at RT is shown in Fig. 6(a) and (b), respectively. For both the samples three isolated peaks are observed. The peaks were assigned in accordance with the previous discussion and are consistent with previous reports [36,38,39]. The peak at about 63.5, 67.5 and 69.5 MHz are assigned to the Fe atoms present at the B-site of Fe_3O_4, the A-site of Fe_3O_4 and (both the sites of) γ-Fe_2O_3 phase, respectively. It is clear from the IFNMR spectroscopy that both the Fe_3O_4 and γ-Fe_2O_3 phases are present in the samples. We have quantified the amount of each phase in each sample by integrating the area under each curve in Fig. 6. The results are tabulated in Table 4. From Table 4 it can be rationalized that the site occupancy of Fe cations in A and B sites of Fe_3O_4 is ~2:1. Furthermore, the sum of the integrated area under all the peaks is 0.62 for the HS2 sample (Fig. 6(a)) and 0.90 for the SS2 sample (Fig. 6(b)). This clearly suggests that the amount of magnetic phases (Fe_3O_4 + γ-Fe_2O_3) in HS2 sample is lower than that of SS2 sample. These results are further verified by the IFNMR measurements at 77 K, which is discussed below.

The internal field of the ferrimagnetic materials largely depends on the temperature; at lower temperature the internal field is higher. The IFNMR spectra measured at 77 K are given in Fig. 6(c, d). Similar to the IFNMR spectra measured at RT, we have observed three peaks each, for both the samples (HS2 and SS2) at 77 K. However, the linewidth of the peaks is high and the peaks are overlapping. The low frequency peaks

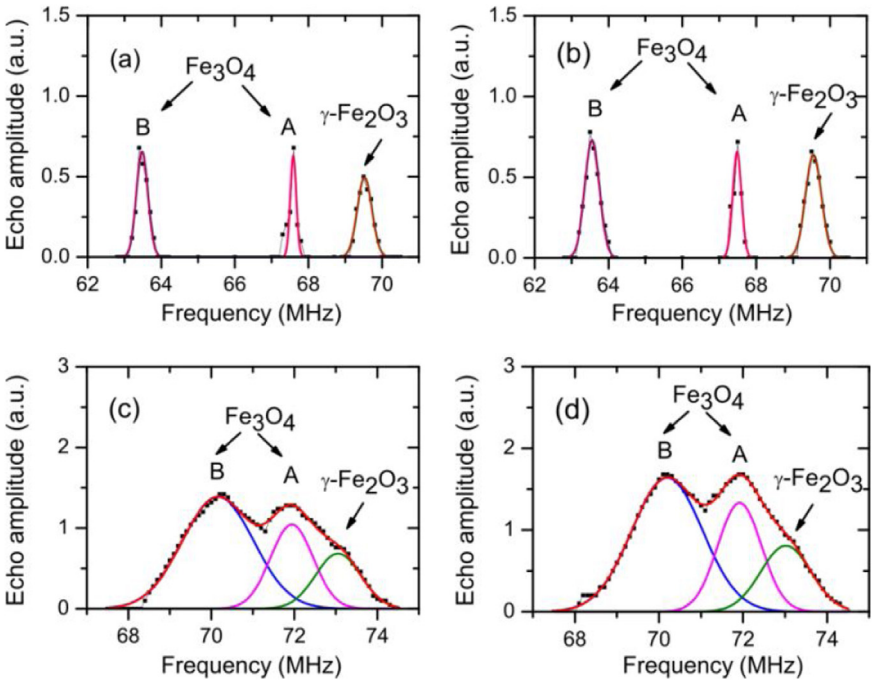

Fig. 6 – The ^{57}Fe IFNMR spectra (echo amplitude versus frequency) of (a) HS2 (b) SS2 samples measured at RT using a two-equal-pulses sequence (1 μs–25 μs–1 μs). The colored lines represent the fitted curves to the measured data points. The ^{57}Fe IFNMR spectra of (c) HS2 and (d) SS2 samples, measured at 77 K using a two-equal-pulses sequence (1 μs–30 μs–1 μs). The blue and pink lines correspond to B and A sites of Fe_3O_4, respectively, and the green lines represent γ-Fe_2O_3. The red line represents the fitted cumulative curve to the measured data points.

Table 4 – NMR parameters obtained from the experiment at two different temperatures (RT and 77 K). Phase composition indicates the magnetic phase; NMR frequency is the center frequency, internal field obtained from the corresponding central NMR frequency. Area is obtained after integrating the NMR frequency curves.

Soil sample	Temperature (K)	Phase composition	Corresponding frequency (MHz)	Internal field (T)	Area in %
HS2	RT	Fe_3O_4 B-site	63.48	45.93	41
		A-site	67.59	48.90	20
		γ-Fe_2O_3	69.53	50.30	39
	77	Fe_3O_4 B-site	70.16	50.62	57
		A-site	71.94	52.12	26
		γ-Fe_2O_3	73.05	52.80	17
SS2	RT	Fe_3O_4 B-site	63.55	45.98	40
		A-site	67.48	48.82	22
		γ-Fe_2O_3	69.55	50.32	38
	77	Fe_3O_4 B-site	69.96	50.62	54
		A-site	72.11	52.17	27
		γ-Fe_2O_3	73.02	52.83	19

at ~ 70 and ~ 72 MHz are assigned to the B-site and A-site of Fe_3O_4 phase and the other peak at ~ 73 MHz is assigned to (both A- and B-sites of) the γ-Fe_2O_3 phase. The origin of the overlapping of the two peaks corresponding to A- and B-sites of Fe_3O_4 is well known in the literature as 'Verwey transition' [40–45]. This corresponds to the transition from metallic to insulating behavior of Fe_3O_4 below the temperature $T_V \approx 122$ K. This change is also associated with a structural transformation from cubic inverse spinel to monoclinic structure. This leads to a change in magnetic properties and both the sites acquiring similar internal field/hyperfine field. As a result, both the peaks, corresponding to A- and B-sites of Fe_3O_4, appear very close to each other as seen in Fig. 6(c, d).

The effect of the local daily temperature on the composition of the soils is described below. Most part of the Hospete is dry-land whereas large part of Sandur includes a forest area. Sandur city is only about 30 km from Hospete. Although, the solar radiation received by both the cities is very similar, the local temperature experienced daily is about 2 °C higher at Hospete than Sandur. Hence, the environmental parameters, e.g., humidity, at both the places are different. Both the cities are known for their iron ore deposits. The soil also contains a high amount of iron-oxide phases. As we see from the above results, the soils collected from both the places contain a very high amount of non-magnetic α-Fe_2O_3 (hematite) along with ferrimagnetic Fe_3O_4 (magnetite)

and γ-Fe_2O_3 (maghemite) phases. However, the α-Fe_2O_3 content in Hospete soil is relatively much higher than that of the Sandur soil.

According to earlier investigations, the ferrimagnetic iron-oxide phases (Fe_3O_4 and γ-Fe_2O_3) transform to stable α-Fe_2O_3 phase between 200 and 350 °C [29]. Fe_3O_4 first transforms to γ-Fe_2O_3 phase between 200 and 250 °C, the γ-Fe_2O_3 phase then transforms to α-Fe_2O_3 between 300 and 350 °C. These transformations are often observed to occur in nature even at lower temperatures, but very slowly depending on the temperature and other environmental conditions.

According to Mössbauer spectroscopy (Fig. 5(a)), VSM (Fig. 5(b)) and IFNMR spectroscopy (Fig. 6) results, the magnetic part of the SS2 sample showed relatively higher amount of magnetic phases (Fe_3O_4 and γ-Fe_2O_3) than HS2 sample. Note that the particles have sizes higher than 1 μm (Fig. 1(i)), hence, the separation of the magnetic and non-magnetic part cannot be done perfectly by a permanent magnet, because, even the finely-ground particles can contain both the phases in the same particle. This is evident from the XRD pattern (Fig. 2(a)) of the non-magnetic parts of the samples (HS1 and SS1). However, this process separates only the magnetic particles that are attracted by the magnet of field strength 1 T. Hence, without losing any generality, we may say that the magnetic parts of the samples contain proportionally higher ferrimagnetic phases. All the results taken together, we observed that the as-collected HS (Hospete) sample has lower amount of magnetic phases (Fe_3O_4 and γ-Fe_2O_3) than that of the as-collected SS (Sandur) sample. Considering that equal amount of iron-oxide phases were created at the beginning (as these two cities, Hospete and Sandur, are close to each other), the rate of transformation of Fe_3O_4 and γ-Fe_2O_3 to α-Fe_2O_3 is higher in Hospete soil than in Sandur soil, because the Sandur soil contains higher amount of ferrimagnetic iron-oxide phases. Hence, the phase composition of the soil is intimately related to the local daily temperature.

4. Conclusion

The structure, elemental composition, phase composition and magnetic properties of two representative iron ores collected from two different regions (Hospete and Sandur) of Karnataka, India, were investigated. Both the samples predominantly contain ceramic phases with Fe and O as the major elements along with a small amount of Al and Si. We found that α-Fe_2O_3 is the dominant phase (~80 wt%) in both the samples. Other iron-oxide phases such as γ-Fe_2O_3 and Fe_3O_4 also constitute the samples along with traces of aluminosilicate (Al_2SiO_5) and low-quartz (SiO_2). Presence of all the iron oxide phases was confirmed by complementary characterizing methods such as XPS, Mössbauer spectroscopy and internal-field NMR spectroscopy. We observed that the soil collected from low temperature region (Sandur) contains more amounts of ferrimagnetic oxide (Fe_3O_4, γ-Fe_2O_3) phases, whereas that collected from the high temperature region (Hospete) contains more α-Fe_2O_3 phase in the soil.

Conflicts of interest

The authors declare no conflicts of interest.

REFERENCES

[1] USGS. Global iron ore production data; clarification of reporting from the USGS. Mın Eng 2017;69:20–3. www.miningengineeringmagazine.com.

[2] Li W, Le C, Qiao L, Zhen J, Yao Y, Liang Y, et al. Electromagnetic interference shielding effectiveness and microwave absorption of ferrite-polymer composite using $Ni_{0.32}Cu_{0.08}Zn_{0.6}Fe_2O_4$. In: Ferrite Prog. Electromagn. Res. Symp. (PIERS). 2016. p. 8–11.

[3] Choudhary HK, Pawar SP, Kumar R, Anupama AV, Bose S, Sahoo B. Mechanistic insight into the critical concentration of barium hexaferrite and the conductive polymeric phase with respect to synergistically electromagnetic interference (EMI) shielding. Chem Select 2017;2:830–41.

[4] Singh K, Ohlan A, Pham VH, Varshney BRS, Jang J, Hur SH, et al. Nanostructured graphene/Fe_3O_4 incorporated polyaniline as a high performance shield against electromagnetic pollution. Nanoscale 2013;5:2411.

[5] Chae HS, Kim SD, Piao SH, Choi HJ. Core-shell structured Fe_3O_4@SiO_2 nanoparticles fabricated by sol–gel method and their magnetorheology. Colloid Polym Sci 2016;294:647–55.

[6] Chand M, Shankar A, Ali N, Jain K, Pant RP, Singh K, et al. Nanostructured graphene/Fe_3O_4 incorporated polyaniline as a high performance shield against electromagnetic pollution. Colloid Polym Sci 2016;5:647–55.

[7] Hlrota K, Suglmura M, Hlrota E. Hot-press ferrites for magnetic recording heads. Ind Eng Chem Prod Res Dev 1984;23:323–30.

[8] Babicheva VE, Zhukovsky SV, Lavrinenko AV. Bismuth ferrite as low-loss switchable material for plasmonic waveguide modulator. Opt Express 2014;22.

[9] Boda SK, Anupama AV, Basu B, Sahoo B. Structural and magnetic phase transformations of hydroxyapatite-magnetite composites under inert and ambient sintering atmospheres. J Phys Chem C 2015;119:6539–55.

[10] Sugimoto M. The past, present, and future of ferrites. J Am Ceram Soc 1999;82:269–80.

[11] Mukherjee S. Applied mineralogy. Netherlands: Springer Publications; 2011.

[12] Petruk W. Applied mineralogy in the mining industry. Netherlands: Elsevier BV; 2000.

[13] Longworth G, Becker L, Thompson R, Oldfield F, Dearing J, Rummery T. Mössbauer effect and magnetic studies of secondary iron oxides in soils. J Soil Sci 1979;30:93–110.

[14] Resende M, Allan J, Coey J. The magnetic soils of Brazil. Earth Planet Sci Lett 1986;78:322–6.

[15] Fabris J, de Jesus Filho M, Coey J, Mussel WN, Goulart A. Iron-rich spinels from Brazilian soils. Hyperf Interact 1997;110:23–32.

[16] Parfitt R, Childs C. Estimation of forms of Fe and Al – a review, and analysis of contrasting soils by dissolution and Mossbauer methods. Soil Res 1988;26:121–44.

[17] Young R. The rietveld method. Oxford University Press: London; 1993.

[18] Rodríguez-Carvajal J. FULLPROF: a program for rietveld refinement and pattern matching analysis. In: Abstr. Satell. Meet. Powder Diffr. XV Congr. IUCr, vol. 127. 1990.

[19] Brand RA. Improving the validity of hyperfine field distributions from magnetic alloys. Nucl Instrum Methods Phys Res Sect B: Beam Interact Mater Atoms 1987;28:398–416.
[20] Brand RA. Improving the validity of hyperfine field distributions from magnetic alloys. Nucl Instrum Methods Phys Res 1987;B28:417–32.
[21] Anupama AV, Manjunatha M, Rathod V, Jali VM, Damle R, Ramesh KP, et al. ^{57}Fe internal field nuclear magnetic resonance and Mössbauer spectroscopy study of Li–Zn ferrites. J Magn Reson 2017;286:68–77.
[22] Siddesh BM, Manjunatha M, Ramakrishna Damle KP. Ramesh, fabrication of low cost and versatile internal field nuclear magnetic resonance spectrometer to study the magnetic materials. Indian J Pure Appl Phys 2018;56:11.
[23] Sawatzky GA, Coey JMD, Morrish AH. Mossbauer study of electron hopping in the octahedral sites of Fe_3O_4. J Appl Phys 1969;40:1402–3.
[24] Greaves C. a powder neutron diffraction investigation of vacancy ordering and covalence in γ-Fe_2O_3. J Solid State Chem 1983;49:325–33.
[25] Anupama AV, Keune W, Sahoo B. Thermally induced phase transformation in multi-phase iron oxide nanoparticles on vacuum annealing. J Magn Magn Mater 2017;439:156–66.
[26] Goss CJ. Saturation magnetisation, coercivity and lattice parameter changes in the system Fe_3O_4-γFe_2O_3, and their relationship to structure. Phys Chem Miner 1988;16:164–71.
[27] Biesinger MC, Payne BP, Grosvenor AP, Lau LWM, Gerson AR, Smart RSC. Resolving surface chemical states in XPS analysis of first row transition metals, oxides and hydroxides: Cr, Mn, Fe, Co and Ni. Appl Surf Sci 2011;257:2717–30.
[28] Payne BP, Biesinger MC, McIntyre NS. Use of oxygen/nickel ratios in the XPS characterisation of oxide phases on nickel metal and nickel alloy surfaces. J Electron Spectros Relat Phenomena 2012;185:159–66.
[29] Uhlig I, Szargan R, Nesbitt H, Laajalehto K. Surface states and reactivity of pyrite and marcasite. Appl Surf Sci 2001;179:222–9.
[30] Li GY, Jiang YR, Huang Kl, Ding P, Chen J. Preparation and properties of magnetic Fe_3O_4–chitosan nanoparticles. J Alloys Comp 2008;466:451–6.
[31] Wang P, Wang X, Yu S, Zou Y, Wang J, Chen Z, et al. Silica coated Fe_3O_4 magnetic nanospheres for high removal of organic pollutants from wastewater. Chem Eng J 2016;306:280–8.
[32] Wang T, Liu Z, Lu M, Wen B, Ouyang Q, Chen Y, et al. Graphene–Fe_3O_4 nanohybrids: synthesis and excellent electromagnetic absorption properties. J Appl Phys 2013;113:024314.
[33] Chen Y, Gao P, Zhu C, Wang R, Wang L, Cao M, et al. Synthesis, magnetic and electromagnetic wave absorption properties of porous Fe_3O_4/Fe/SiO_2 core/shell nanorods. J Appl Phys 2009;106:054303.
[34] Manjunatha M, Kumar R, Sahoo B, Damle R, Ramesh KP. Determination of magnetic domain state of carbon coated iron nanoparticles via ^{57}Fe zero-external-field NMR. J Magn Magn Mater 2018;453:125–31.
[35] Bastow TJ, Trinchi A, Hill MR, Harris R, Muster TH. Vacancy ordering in γ-Fe_2O_3 nanocrystals observed by ^{57}Fe NMR. J Magn Magn Mater 2009;321:2677–81.
[36] Bastow TJ, Trinchi A. NMR analysis of ferromagnets: Fe oxides. Solid State Nucl Magn Reson 2009;35:25–31.
[37] Shim JH, Lee S, Park JH, Han SJ, Jeong YH, Cho YW. Coexistence of ferrimagnetic and antiferromagnetic ordering in Fe-inverted zinc ferrite investigated by NMR. Phys Rev B 2006;73.
[38] Daou TJ, Greneche J, Lee S, Lee S, Lefevre C. Spin Canting of maghemite studied by NMR and in-field Mössbauer spectrometry. J Phys Chem C 2010;114:8794–9.
[39] Lee SJ, Lee S. The spin structure of maghemite investigated by ^{57}Fe NMR. New J Phys 2006;8:1–7.
[40] Tabiś W, Kusz J, Kim-Ngan NTH, Tarnawski Z, Zontone F, Kakol Z, et al. Structural changes at the Verwey transition in Fe_3O_4. Radiat Phys Chem 2009;78:93–6.
[41] Jackson M, Moskowitz B, Bowles J. The magnetite Verwey transition. IRM Q 2011;20:1–11.
[42] Senn MS, Wright JP, Attfield JP. Charge order and three-site distortions in the Verwey structure of magnetite. Nature 2012;481:173–6.
[43] Liu M, Hoffman J, Wang J, Zhang J, Nelson-Cheeseman B, Bhattacharya A. Non-volatile ferroelastic switching of the Verwey transition and resistivity of epitaxial Fe_3O_4/PMN-PT (011). Sci Rep 2013;3:1–8.
[44] Tarnawski Z, Wiecheć A, Madej M, Nowak D, Owoc D, Król G, et al. Studies of the verwey transition in magnetite. Acta Phys Pol A 2004;106:771–5.
[45] Verwey EJW. Electronic conduction of magnetite (Fe_3O_4) and its transition point at low temperatures. Nature 1939;144:327–8.